Dust arriving in the Amazon basin over the past 7,500 years came from diverse sources

Juliana Nogueira, Heitor Evangelista, Claudio de Morisson Valeriano, Abdel Sifeddine, Carla Neto, Gilberto Vaz, Luciane Moreira, Renato Cordeiro, Bruno Turcq, Keila Aniceto, et al.

COMMUNICATIONS EARTH&ENVIRONMENT

ARTICLE

https://doi.org/10.1038/s43247-020-00071-w OPEN

Dust arriving in the Amazon basin over the past 7,500 years came from diverse sources

Juliana Nogueira[1✉], Heitor Evangelista[1], Claudio de Morisson Valeriano[2,3], Abdelfettah Sifeddine[4], Carla Neto[2], Gilberto Vaz[2], Luciane S. Moreira[5], Renato C. Cordeiro[5], Bruno Turcq[4], Keila Cristina Aniceto[6], Artur Bastos Neto[7], Gabriel Martins[5], Cybelli G. G. Barbosa[8], Ricardo H. M. Godoi[8] & Marilia H. Shimizu[9]

A large amount of dust from the Sahara reaches the Amazon Basin, as observed with satellite imagery. This dust is thought to carry micronutrients that could help fertilize the rainforest. However, considering different atmospheric transport conditions, different aridity levels in South America and Africa and active volcanism, it is not clear if the same pathways for dust have occurred throughout the Holocene. Here we present analyses of Sr-Nd isotopic ratios of a lacustrine sediment core from remote Lake Pata in the Amazon region that encompasses the past 7,500 years before present, and compare these ratios to dust signatures from a variety of sources. We find that dust reaching the western Amazon region during the study period had diverse origins, including the Andean region and northern and southern Africa. We suggest that the Sahara Desert was not the dominant source of dust throughout the vast Amazon basin over the past 7,500 years.

[1] LARAMG/DBB/IBRAG, Rio de Janeiro State University, Rio de Janeiro, Brazil. [2] LAGIR/FGEL, Rio de Janeiro State University, Rio de Janeiro, Brazil. [3] TEKTOS Research Group, Rio de Janeiro, Brazil. [4] Center IRD France-Nord, IRD-Sorbonne University, (UPMC, Univ. Paris 06) - CNRS/MNHN, LOCEAN Laboratory, Bondy, France. [5] Department of Geochemistry, Fluminense Federal University, Niterói, Brazil. [6] Postgraduate Program in Geosciences, Federal University of Amazonas, Manaus, Brazil. [7] La Salle University, Canoas, Brazil. [8] Department of Environmental Engineering, Federal University of Paraná, Curitiba, Brazil. [9] Center for Weather Forecasting and Climate, Studies, National Institute for Space Research, São Paulo, Brazil. ✉email: junogueira@id.uff.br

Mineral dust plays an important role both in the climate system[1] and in the maintenance of ecosystems through the biogeochemical interactions of macro and micronutrients that fertilize the oceans and continents[2–11]. Arid and semi-arid regions are the main global dust sources, where particles can be lifted into the atmosphere, transported, and deposited far away from their sources[12]. Once it has been accumulated in lake sediment layers, dust acts as an archive of past atmospheric dynamics, and thus, dust is likely to give information about the arid conditions in its source areas and the associated atmospheric circulation patterns[13–15].

Many authors suggest that Saharan dust contributes considerably to fertilizing the Amazon rainforest through nutrient exportation[10,16,17]. Nevertheless, due to uncertainties from limited existing geochemical databases of Fe (II), Fe (III), and P, and precise estimates of atmospheric fluxes, causal relationship is not fully supported[10,11,17–19]. Some authors claim that an association between Saharan dust dispersion and the development of the rainforest exists based on remote sensing evidence, which is a modern view. However, dust advection to the Amazon basin through time has changed due to shifts in the Intertropical Convergence Zone (ITCZ) and "Saharan green phases"[20,21]. It is reasonable that Saharan dust may impact the eastern Amazon sector considering its close proximity and initial evidence[10,22–24].

Nevertheless, since the Amazon rainforest covers a vast area of 5500000 km² (between approximately 50°W and 80°W longitude and 5°N and 17°S latitude), herein we investigate whether a Saharan dust signal/fingerprint is measurable in the greatly distant region of the central-western Amazon sector during the Holocene. To achieve this, we drilled a sediment core (hereafter denoted as the LPTV-09 core) at one of the most remote, pristine, and isolated locations of the Amazon region, the Lake Pata (LP) (Fig. 1). Lake Pata is situated 300 m above sea level and is part of the Seis Lagos hill lacustrine complex, an inselberg capped by a ferruginous lateritic crust (Supplementary Fig. 1). As it is not connected to any important drainage system, the lake constitutes a nearly isolated system in terms of atmospheric precipitation and dust accumulation, apart from local lateral inputs. According to Köppen classification, the regional climate of Lake Pata is classified as equatorial (Af)[25,26]. The nearest weather station is located in the town of São Gabriel da Cachoeira, 20 km away from Lake Pata. Climatic data from 1961 to 2018 were provided by the Brazilian National Institute of Meteorology (INMET) and can be found at http://www.inmet.gov.br. During this period, the minimum recorded annual rainfall was 2201 mm (1986), the maximum was 3532 mm (1967), and the average annual rainfall was 2965 mm. The wet season ranges from mid-December to mid-May (with an average rainfall of 1697 mm), and the drier season (although not evident) occurs during August–November (with an average rainfall of 757 mm). Due to its privileged location, with a high degree of continental isolation and very low human impact, Lake Pata can be considered a sensitive archive of the equatorial paleoclimate, as previously suggested by palynological and geochemical studies[27–37].

Several works indicate mineral dust composition and mineralogy as reliable proxies for atmospheric circulation and dust-emitting sources[13,38]. Current methods include a combination of geochemical fingerprints and numerical models to identify potential emission sources. Among them, the radiogenic isotope composition of dust particles has been used as a robust method to search for provenance[39]. The isotopic ratios of Sr and Nd in the crust are clearly different from those in the mantle, allowing their lithological origins to be distinguished[39]. Two ratios are commonly used: $^{87}Sr/^{86}Sr$ and $^{143}Nd/^{144}Nd$, where ^{87}Sr is a decay product of ^{87}Rb, a long-lived radionuclide (half-life $= 4.88 \times 10^{10}$ years) and ^{143}Nd derived from ^{147}Sm (half-life $= 1.06 \times 10^{11}$ years). These nuclides are used as conservative fingerprints of sediment and dust provenance for the Pleistocene[14,40], Holocene[41], and modern

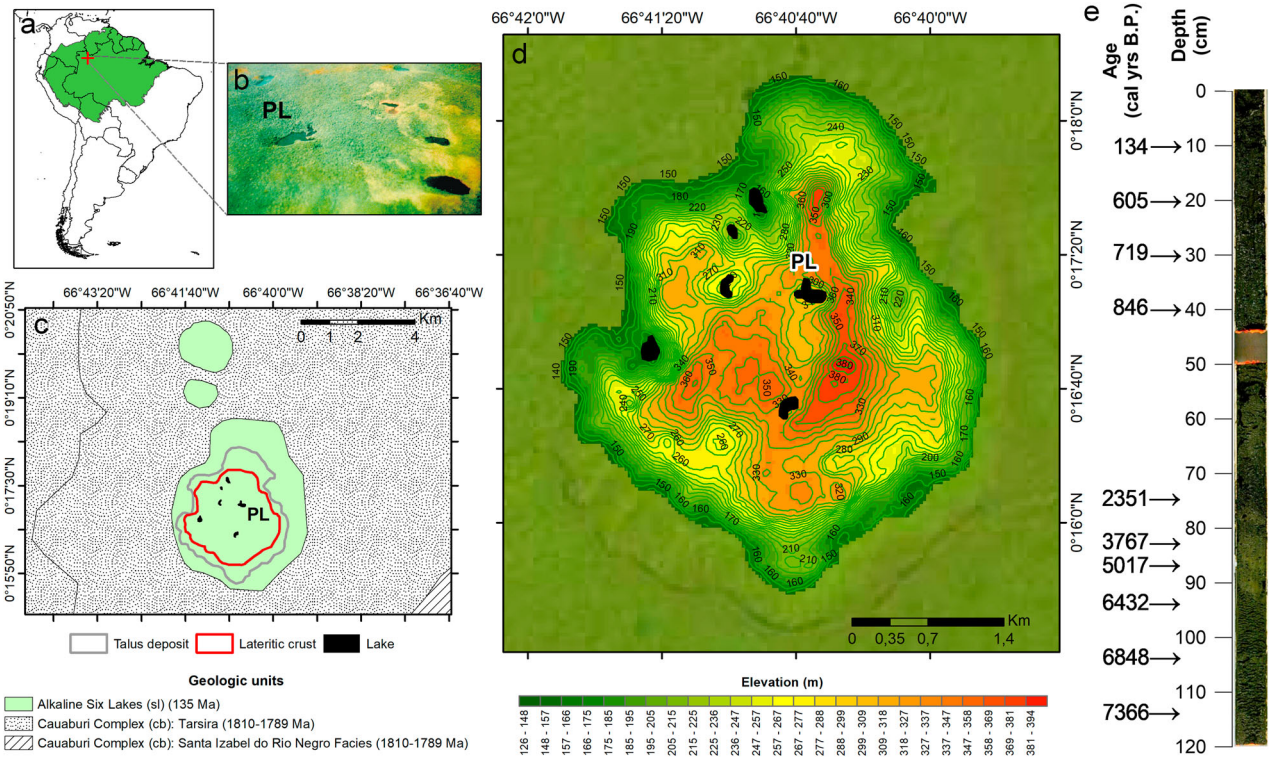

Fig. 1 Lake Pata geographical and geological characterization. a Lake Pata location (0°17′9.68″N, 66°40′36.18″W) in the Amazon rainforest (domain based on GeoServer/Harvard University). **b** Aerial photography. **c** Geological domains for the study areas highlighting the Alkaline Six Lakes, dating to 135 Ma. **d** Hypsometric representation of Seis Lagos hill. **e** Lacustrine sediment core LPTV-09 and its age in calibrated years before present.

timescales[42]. In this way, these isotopic ratios may reflect the geological origins of the terrigenous aerosols being transported in the atmosphere[39].

Precipitation and long-range dust transport to the Amazon basin are constrained by the positioning and intensity of the ITCZ, a low-pressure zone located around the equator where the northeast and southeast trade winds converge.

Due to the higher solar radiation levels near the equator, the air is forced to rise to the upper troposphere along the ITCZ, where it moves towards higher latitudes and slowly descends, leading to large high-pressure areas in the subtropics. The latitudinal position if the ITCZ varies seasonally. In South America, it is located in its southernmost setting during austral summer, causing high precipitation over the Amazon basin. In this season, Lake Pata remains under the influence of the ITCZ, causing its maximum water levels. Its minimum water levels are recorded during austral winter, when the ITCZ migrates northward, reducing the amount of precipitation falling in the region[43].

Seis Lagos hill is part of a Cretaceous carbonatite complex in which sediments were intensively modified due to the substantial local weathering. It is capped by a lateritic crust rich in rare-earth elements exceeding 200 m in thickness[31]. The original ferrocarbonatite, which is rich in Sr, is only detectable below 230 meters. The lake water level varies according to precipitation and possibly never overflow due to percolation through fractures and voids in the laterite[31]. Additional geological details of the site are provided in Supplementary Fig. 1.

In this work, we compiled a comprehensive Sr–Nd isotope database comprising the most important potential emission sources from Africa and South America, including Andean volcanic zones and Patagonia to compare their signatures with those of Lake Pata Holocene sediments, which encompass the last 7500 years. The results presented will demonstrate that, given the complexity of dynamic climatic factors during the Holocene, and the different climatic conditions in both the Amazon rainforest and the potential dust sources, the Saharan dust impact cannot be generalized as the main source for the entire Amazon rainforest and that other dust source regions have important contributions.

Results

Atmospheric scenarios for long-range dust influx at Lake Pata. To recognize the atmospheric circulation patterns that could favor dust reaching Lake Pata, we used the Lagrangian HYSPLIT (HYbrid Single-Particle Lagrangian Integrated Trajectory)/NOAA (National Oceanic and Atmospheric Administration) model[44,45]. This model allows the investigation of air mass migrations and has been successfully used for aerosol dispersion[46–49]. Here, we used monthly backward air mass trajectories at a mid-boundary layer height for the last 30 years, with Lake Pata as the endpoint. The set of superimposed trajectories reveals three main patterns and associated potential sources: from December to April, air masses are predominately from North Africa and the Sahara/Sahel region; from July to September, two different source regions, southern Africa (primarily) and the eastern Andes, were detected; and transitions period from May to June and October to November show air masses advecting from both northern and southern sources. As expected, due to the equatorial location of the lake, these patterns are modulated by the position of the trade winds[10,22,43,50,51].

During austral winter, when the ITCZ is located farther north, both the South Atlantic Anticyclone[52] and the cold front frequency[53] are notably stronger. In South America, during austral winter, air masses advection along the eastern Andean face, coming from subtropical and subpolar latitudes, frequently reach western Amazonia, as represented in Fig. 2. This migration corridor, typical of the austral winter months of July and August, characterize a phenomenon known as "*friagem*"[54], that causes the most pronounced air temperature decrease in the Amazon basin. North African advections take place between December and April, which corresponds to the Amazonian wet season. Currently, dust advection from the Sahara to the Amazon basin takes place under two competing conditions: (1) a maximum dust load to the Amazon basin due to the large desert region; and (2) prevailing moisture conditions in the Amazon basin that may favor dust deposition from the easter to western Amazon basin due to the precipitation distribution that encloses the entire hydrological basin. Therefore, dust dispersion is constrained to more inland advections as a result of a washout along with air mass migration.

Methodology validation. To test Sr and Nd isotopic ratios as dust fingerprinting methods, and therefore their usefulness in tracking the origin of the air masses in the Amazon basin, we conducted a validation experiment based on atmospheric sampling in the Amazon basin. Sampling sessions were held in the facilities of the Amazon Tall Tower Observatory (ATTO), located 150 km north of Manaus city. We analyzed aerosols collected at 80 m above the ground in two campaigns: one during the wet season and one during the dry season. The total aerosol fraction was collected in a quartz filter (during the 2013 dry season), and a 2.5 µm cutoff was used for particulate matter in polycarbonate filters (during the 2012–2013 wet season). Each campaign provided blanks for analysis (Supplementary Table 1). Sr and Nd isotopic ratios were measured through a thermal ionization mass spectrometer (TIMS). For the corresponding sampling period, air mass backward trajectories were obtained with the HYSPLIT/NOAA model. In parallel, we constructed a comprehensive Sr–Nd isotope database (containing 253 entries) of potential dust-emitting sites indicated by the trajectory model, as displayed in Fig. 2 (Fig. 3a and Supplementary Data 1). Additionally, to infer the dust activity at potential dust-emitting sources, we used the Aerosol Index (OMTO3d v003 – GIOVANNI/NASA) (Fig. 3b, c). Coupling the air mass backward trajectories and the Aerosol Index spatial distribution, it was possible to identify the most likely dust source regions, as depicted in Fig. 3d. During the sampling period, the ATTO tower was under the influence of two major potential dust-emitting sources: the Sahara/Sahel sector and southern Africa. Nd isotopic ratios, represented as εNd (0), in the aerosol samples collected in January and September changed considerably (from −6.3 to −12.3) corresponding to changes in the patterns of the air mass backward trajectories and their corresponding dust activity areas (Supplementary Table 2). Comparing our aerosol data with the isotopic inventory, it is clear that the εNd (0) parameter effectively distinguishes the southern African dust signature from the Sahara/Sahel pattern. A full description of this method is described in the literature[55]. For the time periods of the experiments conducted at the ATTO, the Sr isotope data derived from mineral dust were too low to be detected after the removal of the seawater component.

Sr–Nd isotopes of the Lake Pata sediment core. The complete Sr–Nd isotope database of this work ($n = 27$), which comprises the core sediments and the hill lateritic crust, is presented in Fig. 4 (Sr–Nd isotope data, with errors, corresponding to their respective core depths are presented in Supplementary Data 2). The chronological model for the LPTV-09 core is shown in Supplementary Table 3 and Supplementary Fig. 2. The core spans the period from 2014 to 7366 years B.P. The Lake Pata sediment core exhibits a narrow isotopic limit, where εNd (0) varies between −0.4 and 1.2, while the $^{87}Sr/^{86}Sr$ ratio ranges from 0.711021 to

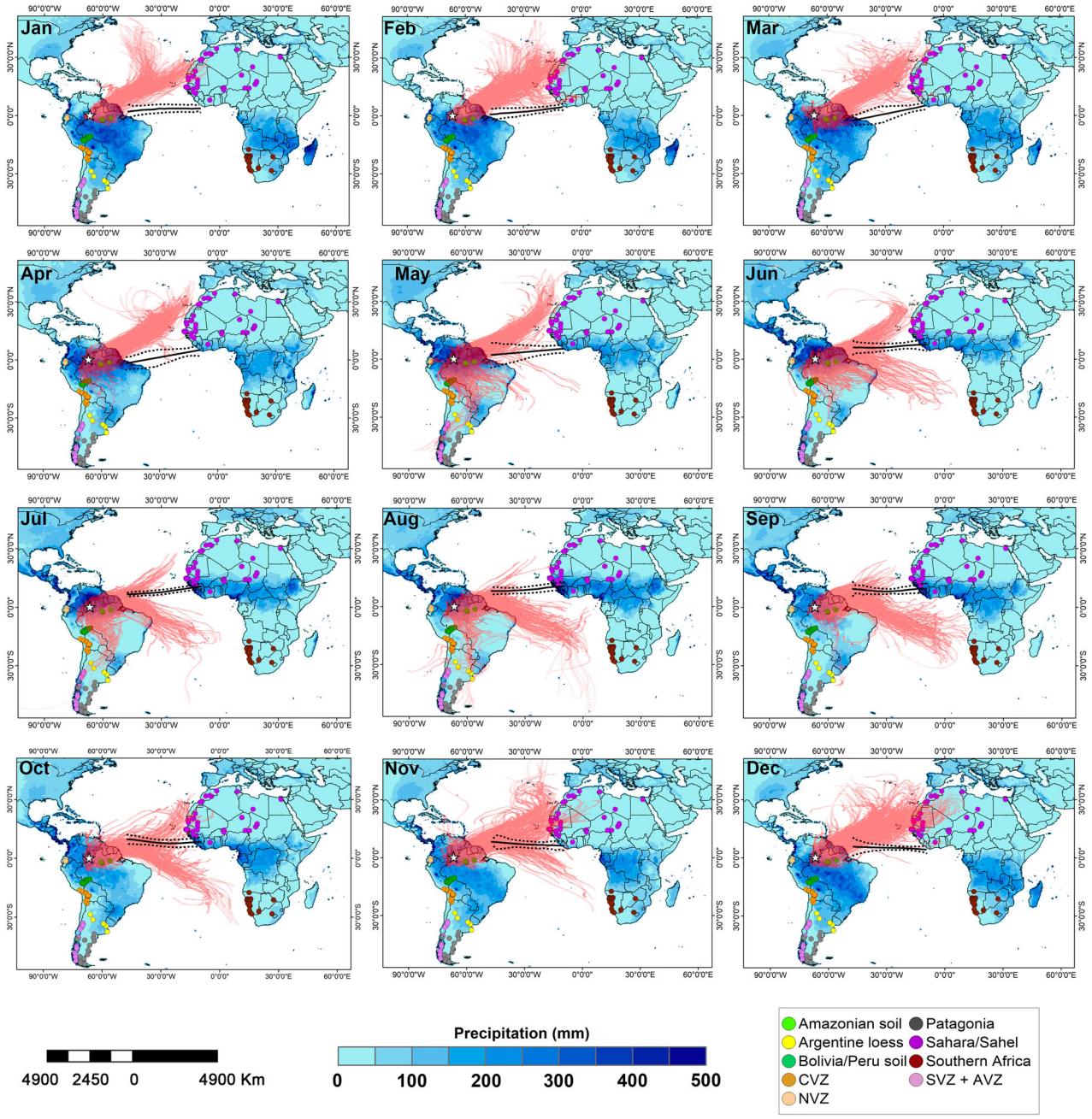

Fig. 2 The current climatology of air masses arriving at Lake Pata along with precipitation, ITCZ dynamics, and potential dust source areas. Backward air mass trajectory for the last 30 years reaching Lake Pata (red lines). The star indicates the location of Lake Pata, and the black continuous and dashed lines represent the ITCZ historical average and 2σ standard deviation, respectively, modeled for the period between 1975 and 2013 based on OLR data[102]. The blue colors over the continents represent the annual precipitation pattern based on GPCC Precipitation 0.5 degree monthly long-term mean V2018 Full Reanalysis database for 1891 to 2016 (http://gpcc.dwd.de/)[103].

0.711859. For the lateritic crust of Seis Lagos hill, which includes the lake bed, εNd (0) varies from −0.4 to 0.6, and the $^{87}Sr/^{86}Sr$ ratio varies between 0.706564 and 0.712375, reflecting the juvenile, mantle-derived character of the complex. This is quite similar to volcanic ash isotopic signatures—from the Andean Central Volcanic Zone (CVZ), the Northern Volcanic Zone (NVZ), and the Southern Volcanic Zone (SVZ) + the Austral Volcanic Zone (AVZ)—and from the southern South America region, the Patagonia and Argentine loess—characterized by high εNd (0) and low $^{87}Sr/^{86}Sr$ ratios. On the other hand, intensively reworked soils from the Amazon, Sahara, and Sahel regions display higher $^{87}Sr/^{86}Sr$ ratios and more negative εNd (0), which are related to their older geologic ages. In contrast, and more comprehensively, southern African soils present a wide isotopic range, displaying both juvenile and crustal sediment signatures.

In the Sr–Nd isotopic diagram (Fig. 4 and Supplementary Fig. 3), the Lake Pata data appear partially embedded in the domain of several sources as a result of more than one isotopic contribution, despite the strong influence of the local lateritic crust. The Lake Pata sediments are a mixture of eroded material lateritic from the crust that enters the lake by runoff and atmospheric dust deposits. The geomorphology and the uniform lithology of Lake Pata favor a near-constant sediment isotopic signature supply. This characteristic is evidenced by the analysis

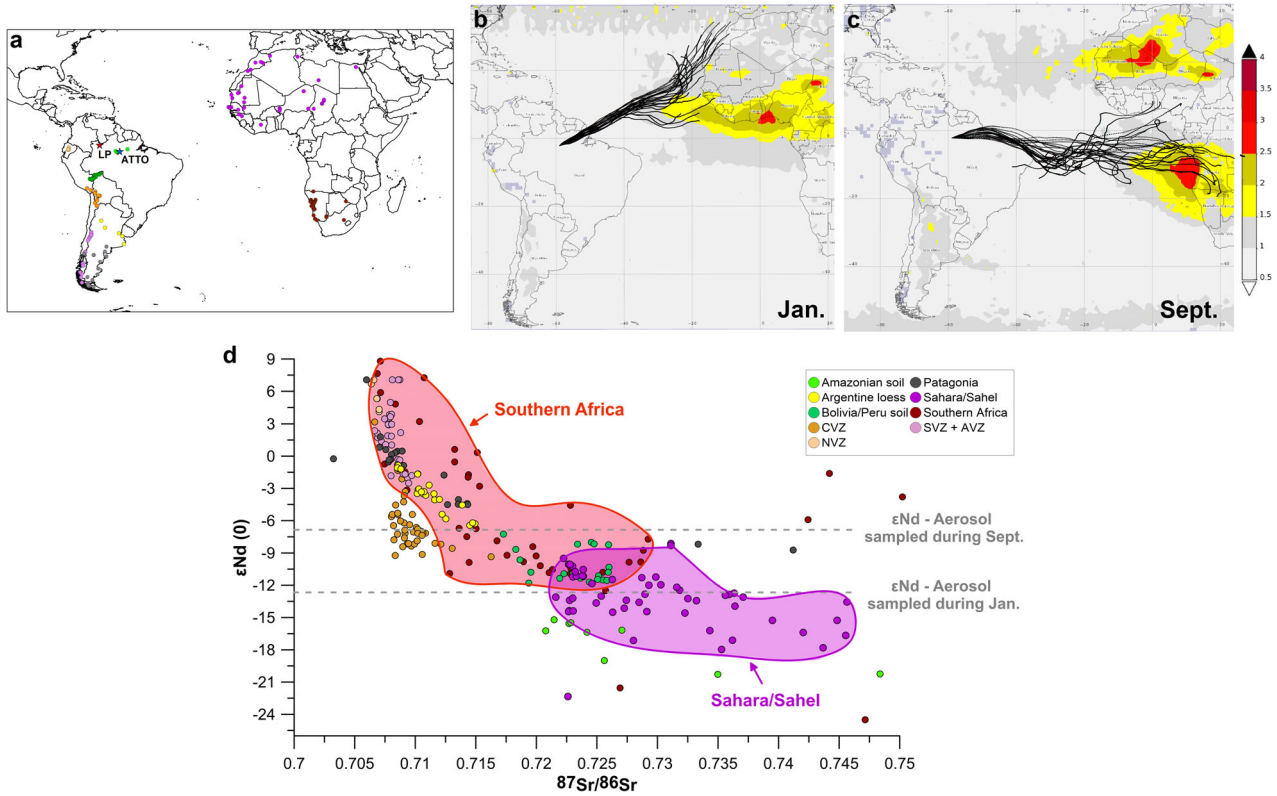

Fig. 3 Methodological validation comparing radiogenic isotopes measured in aerosol filters in the eastern Amazon with active dust-emitting sources and backward air mass trajectories for the sampling period. a Potential source areas for dust exportation along with Lake Pata (LP, red star) and the ATTO (blue star) locations. **b**, **c** represent the Aerosol Index data and the backward trajectories for the ATTO sampling period of January and September, respectively. **d** Comparison between the εNd (0) from air dust filters from January and September at the ATTO—gray dashed lines—and potential sources. Areas in red and purple represent the isotope domain for South Africa and the Sahara/Sahel regions, respectively, according to potential dust sources inferred from the data shown in **b** and **c**. Note: The sea salt Sr imprint was not removed, and the discrimination was based only on the Nd isotope data.

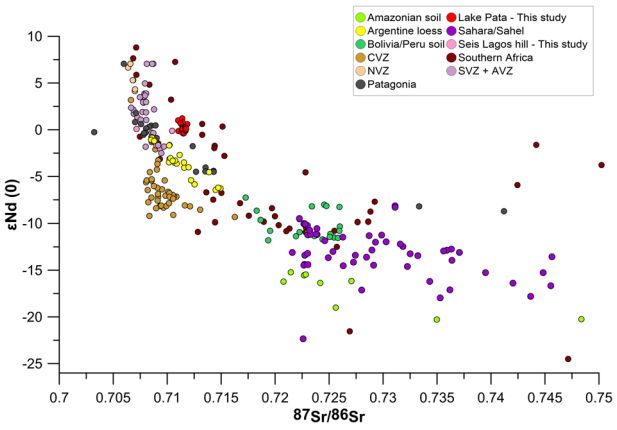

Fig. 4 Sr and Nd isotopic ratios for potential source areas and Lake Pata and Seis Lagos hill (this study). Errors bars for the generated data are not visible in this scale but are provided in Supplementary Data 2 and Supplementary Fig. 3.

of lateritic crust samples with standard deviations of 0.000007 for εNd (0) and 0.002329 for Sr isotopic ratios. Therefore, the recognition of an exogenous atmospheric contribution in the sediment composition was based on the deviations observed from the lateritic crust signal, which are taken as baseline data.

Sediments from different sources with specific radiogenic signatures result in a "mixed signature" material when naturally mixed. However, if the elemental concentrations and radiogenic isotopic for both Sr and Nd are known, then for each source term, it is possible to infer their contribution by using the classic binary mixing model and applying Faure's equation[56] (Fig. 5 and Supplementary Data 3, 4). Using this method, we established the Seis Lagos hill laterite as a fixed end-member and used the postulated dust source contributors as the second extreme. Isotopic mixing curves are expressed by hyperbolic functions linking the mean values of the postulated sources. To be more accurate in searching for mixing percentages, we employed hyperbolic functions for the regions indicated by the backward trajectories in Fig. 2 both for the average isotopic values and for the entire range of the existing data at each domain, obtaining the minimum, average and maximum mixing probabilities. In this way, we evaluated all potential emitting regions individually, that is (1) the Sahara/Sahel sector; (2) Southern Africa; (3) Bolivia/Peru; (4) Patagonia, and (5) the Argentine loess.

Our results suggest that the atmospheric deposition of long-range dust material from arid/semi-arid zones occurred during the mid-to-late Holocene in central-western Amazon in measurable amounts. These dust materials were derived from sources in the Sahara/Sahel, southern Africa, Bolivian/Peruvian soils, and the Argentine loess. Mixture levels varied from ~4 to 10% for the Sahara/Sahel sector, ~8 to 11% for Bolivian/Peruvian soils, ~10 to 50% for southern Africa, and 13 to 15% for the Argentine loess. Although the Patagonia region was initially assumed to be a potential source based only on the modeled atmospheric dynamics, no isotopic signal of such a component was detected for the long-term.

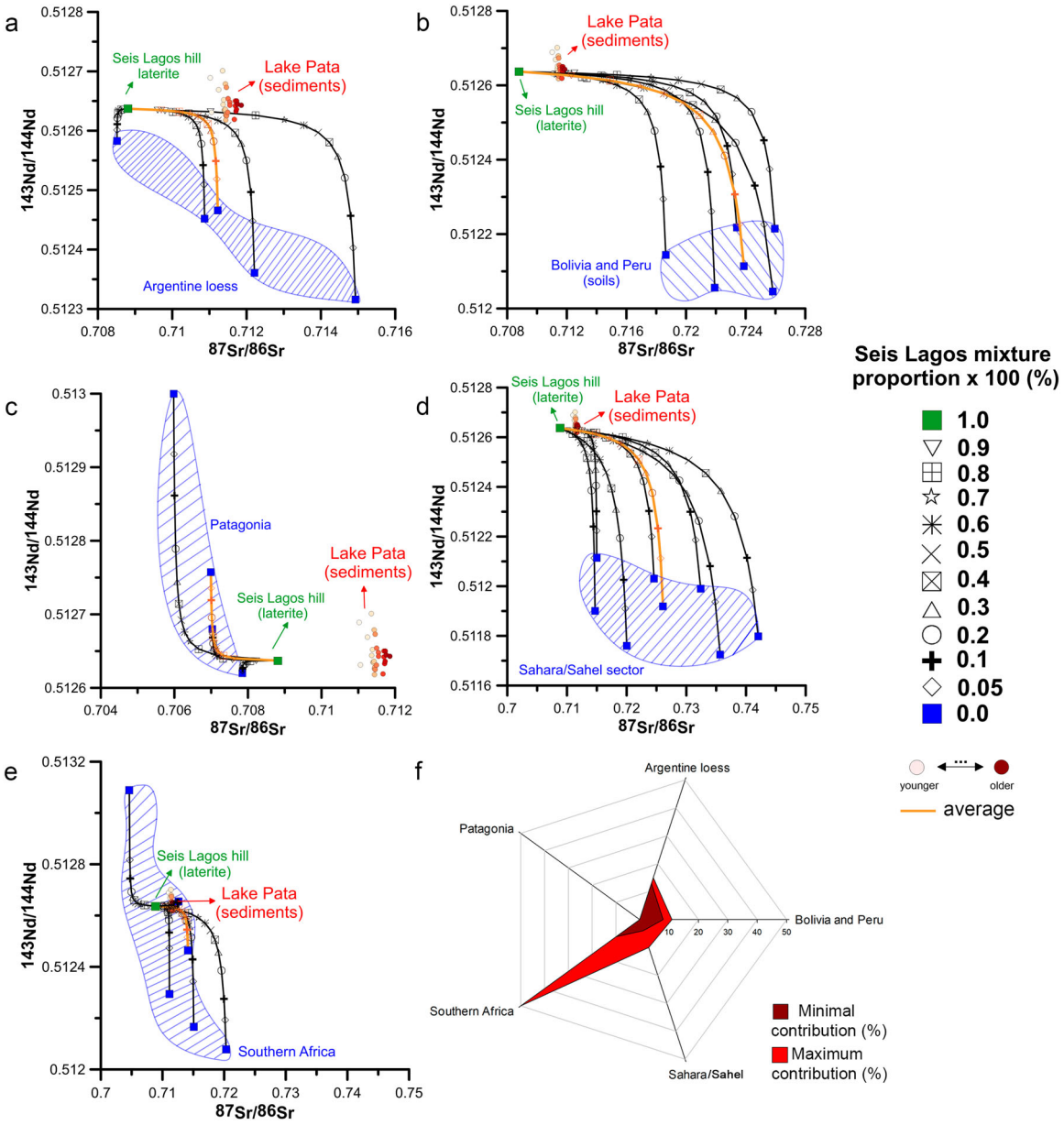

Fig. 5 Binary mixing curves56 between the Seis Lagos hill lateritic crust, where Lake Pata is inserted, and the different possible dust sources. **a** Argentine loess, **b** Bolivian/Peruvian soils, **c** Patagonia, **d** Sahara/Sahel sector, and e southern Africa. The diagram in **f** summarizes the minimum and maximum estimated contributions for each area, indicating a mixture between the Seis Lagos hill laterite signal with contributions of ~4–10% for Sahara/Sahel sector, ~8–11% for Bolivian/Peruvian soils, ~10–50% for Southern Africa, and 13–15% for Argentine loess.

Discussion

The northerly air advections that take place in southern South America during the austral winter season (July–August in Fig. 2) are known mechanisms associated with polar cold fronts that reach the western Amazon region and they are potential mechanisms that transport dust to the western Amazon region since they originate in the neotropical (primary and reworked) loess domain, which covers a large part of Argentina north of 30° S. Additionally, due to the proximity of Andean bare soils to the western Amazon basin, a signal of this site was evident at our study site.

One interesting finding arising from our work is that, contrary to many reports that claim the Sahara Desert as the unique source of dust reaching the Amazon basin[10,16,17,19,22,24,57,58], our data depict a more complex scenario. On long-term timescales, the sedimentary record at Lake Pata points to African deserts, both north and south, soils of the central Andes, and Argentine loess as potential contributors, with southern Africa being even more important than the Sahara Desert for this sector of the Amazon basin during the mid-to-late Holocene.

In addition to the use of radiogenic isotopes to identify dust sources, the Holocenic changes in the εNd at Lake Pata are also important in this context. The εNd data show that 55% of our database falls below the 95% confidence level of the local lateritic isotopic imprint, which may indicate an atmospherically-derived inflow. The εNd values presented in Fig. 6b tend to be higher after 4 kyr B.P., suggesting the influence of a persistent mixture of more juvenile sources (with higher εNd values). From the postulated sources investigated in this study, this influence could be derived only from southern Africa, the NVZ, the SVZ, and the AVZ, as depicted in Fig. 4. The literature reports juvenile values of εNd for ash material from several volcanic events[59]. Therefore,

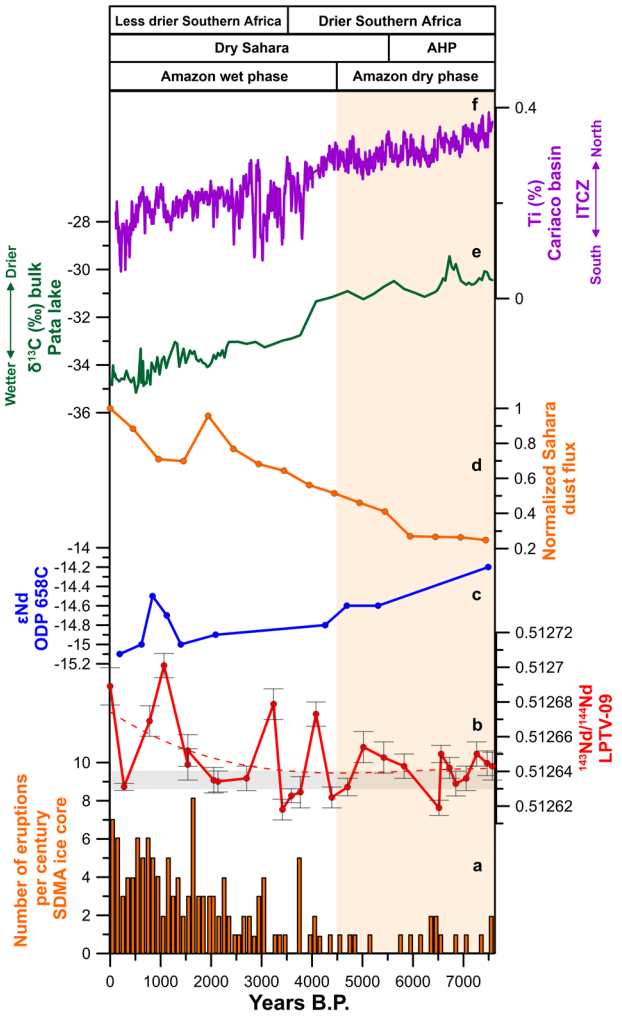

Fig. 6 Multiproxy comparison outlining the aerosol exportation scenario and paleoclimatic conditions on the central and southern Atlantic sectors. a Number of eruptions per century recorded at the SDMA ice core in Marie Byrd Land (West Antarctica)[60]; **b** $^{143}Nd/^{144}Nd$ data of Lake Pata with its error bars. The dashed red line represents the data trend. The horizontal gray bar represents the Seis Lagos hill crustal isotopic signal; **c** εNd data of a marine sediment core from the North African continental shelf[61]; **d** Normalized Saharan dust flux modeled based on the previous publications[5,63,64]; **e** $\delta^{13}C$ from Lake Pata bulk sediment[29]; **f** Ti concentration in the Cariaco Basin[20]. AHP African Humid Period. The vertical red bar represents the Amazonian dry period.

one explanation for the continuous increase in εNd is the influence of the Andean, and probably global, volcanic impact. To evaluate the consistency of this hypothesis, we compared the εNd time series with a detailed volcanic record time series, retrieved from the Antarctic ice core at the WAIS (West Antarctica Ice Sheet) Divide/Marie Byrd Land[60], which details the time sequence of major volcanic eruptions. Many of the volcanic events that comprise the ice core database[60] refer to Chilean volcanic eruptions and therefore potentially impact the Amazon basin. Figure 6a depicts a very similar trend between the number of eruptions recorded in Antarctica per century and the εNd values at Lake Pata since the mid-Holocene (Fig. 6b). Additionally, from a time perspective, we compared the εNd values of Lake Pata with those of the Eastern Atlantic ODP 658C sediment core[61], which is representative of mixed northern African dust sources (Fig. 6c). In this case, the African radiogenic signature tends toward progressively more negative values with time. This behavior clearly contrasts with the increasing trend of εNd values observed at Lake Pata, even though this period represents the humid-dry transition between the humid phase and drier phases of the Sahara Desert[62].

Simplified estimation of the total Saharan dust load at Lake Pata since the mid-Holocene is presented in Fig. 6d (for details, see Supplementary Fig. 4). To estimate the dust flux reaching Lake Pata from the Saharan within the last 7.5 kyr B.P., we have proposed a linear method using the relationship between modeled dust flux at the African margin ocean surface, close to the Sahara Desert (averaging three model outputs for the modern dust flux[5,63,64]) and modern dust deposition at the sea bottom[65] for the corresponding site. Dust fluxes for sections of the sediment cores for 6 yr B.P. and the Last Glacial Maximum (LGM) were also taken into account and compared with modeled dust flux[64] at 6 kyr B.P. and the LGM[63]. The estimation suggests that the Saharan dust flux to Lake Pata during the mid-Holocene decreased up to five times compared to the present contribution, which is coincident with the African Humid Period (14.8–5.5 kyr B.P.)[66]. Time series "e" and "f" in Fig. 6 show that the Cariaco basin possesses the opposite hydrological regime in comparison to the Lake Pata site. The decreasing $\delta^{13}C$ values at Lake Pata are related to wetter conditions[29], while the decrease in Ti (%) in the Cariaco basin is related to drier conditions[20]. Thus, during the mid-Holocene drought event in the Amazon basin[27,67–70] between ~7.5 and 4.5 kyr when the Atlantic ITCZ was slightly displaced to the north[71,72], the lateral sediment flux at Lake Pata reached a minimum.

Variations in the local isotopic signal in our data suggest a mixture of different dust sources reaching Lake Pata. Potential dust sources were postulated taking into consideration (1) the observation of favorable conditions related to atmospheric transport between the arid region and the central-western Amazon, (2) the relative intensity of dust emissions at the sources, and (3) the local climatic conditions at Lake Pata as favorable conditions for dust deposition. Between 7.5 and 5.5-4.5 kyr B.P., wet conditions prevailed in northern Africa[73–75] and, thus, its importance as a potential dust source area is limited[65]. During this period, few deviations from the local εNd isotopic signature were observed for Lake Pata, indicating few contributions from any allochthonous source. Additionally, although drier conditions prevailed in southern Africa until ~3.5 kyr B.P.[76–78], the increase in the meridionality of the trade winds[79,80] caused inefficiency in the transatlantic transport of dust exported by that area, as also indicated by the wind vectors derived from simulations from CMIP5 multi-model (Supplementary Fig. 5). For the austral summer mid-Holocene simulations from this model, it is also possible to see a predominance in advections coming from southern South America, contrarily to what it is observed during the modern period when air mass come predominantly from northern Africa.

After 4.5 kyr B.P., increases in the trend and variability of εNd values are observed, indicating an intermittent contribution of other sources to the lake, such as the ones depicted in Fig. 5f (Argentine loess, Bolivian and Peruvian soils, Sahara/Sahel sector and southern Africa). Wet conditions characterize the Amazonian hydrology during the late Holocene as a consequence of the southward shift, expansion, and intensification[20] of the Atlantic ITCZ, as well as an enhanced South American Monsoon System (SAMS). During the same period, the Sahara became a well-established dust source, similar to the modern scenario that would be favorable to the delivery of dust. However, the Saharan εNd fingerprint (as recorded from the ODP 658C sediment

core[61]) tended to become more negative with time in contrast to the Lake Pata isotopic imprint.

From the several paleorecords comparing the climate variabilities of the Central Amazon basin and Cariaco basin[81–83], it is evident that the ITCZ latitudinal shifts and width variations modulate the dry and wet climate regimes in the Amazon basin. In this context, trade wind positioning influences the amount of dust being transported from the Sahara to the Amazon basin. In the Holocene scenario, the present-day ITCZ position is compared to the south, which explains the actual wet conditions observed in most of the Amazon hydrological basin[20].

The issue of the Sahara Desert fertilizing the Amazon basin has been discussed for decades. Nevertheless, there has never been a consensus. The *terra firme* dense tropical rainforest covers the majority of this region and is characterized by its soils with low natural chemical fertility. For fertilization, vegetation relies mainly on the recycling of local organic matter and on nutrient input through both wet and dry deposition[84,85]. In this sense, Reichholf[11] and Swap et al.[10] claim that the emergence and development of the Amazon rainforest have been influenced not only by changes in the amount of local precipitation but also by the atmospheric nutrient influx to the basin. Research on the atmosphere over the Amazon basin encompasses its composition and physical and chemical processes[86–89]. Currently, northern Africa is believed to be the origin of the air masses that bring such nutrients. However, these assumptions are based mainly on satellite images and dispersion models, with few in situ measurements or specific geochemical signatures indicating their origins[10,11,19,22,90]. Yet, when analyzing surface material in the northeastern Amazon basin, Abouchami et al.[1] did not find a Sahara fingerprint.

In this work, we do not rule out the Sahara dust as an important player in the fertilization of the Amazon rainforest. However, in our study, we show that this relationship is probably not valid for the entire hydrological basin, since, although there is a residual fingerprint of Sahara dust, other sources, such as southern African and Argentine loess, seem to be more dominant for more continental inland portions of the Amazon basin. Previous works address the fertilization issue only on the basis of a modern database[19,90] and do not consider the fact that the rainforest evolution dates as far back as the Pleistocene, including periods when the Sahara was greener than it is today (the African Humid Period) and when a load of dust reaching the Amazon basin was much lower[21]. Herein, we do not discard the possibility that fertilization occurs at sites closer to the Atlantic Ocean, subject to a higher dust load[16,91]. We base our conclusions on a Holocene analysis of Sr–Nd isotopic ratios as tracers of dust provenance. More recently, daily measurements of mineral dust and PM10 carried on trade winds between 2002 and 2017 in French Guiana indicated that the deposition rates in the Amazon basin, although significant, are substantially smaller than rates from the previous studies[92]. In this sense, the deposition rates are greater over the northern and northeastern regions of South America and lower in central Amazonia; this behavior is attributed to the wet removal of dust during transport through the rainy regions of the ITCZ.

In contrast to the modern high dust loads reaching the eastern Amazon basin, from the isotopic method, we have estimated smaller contributions of the Sahara/Sahel dust signal during the last 7.5 kyr B.P., ranging from ~4 to ~10%. Contributions from southern Africa (~10–50%), Bolivian/Peruvian soils (~8–11%), and, finally, Argentine loess (~13–15%) also accounted for the isotopic signal at western Amazon. It is also possible that dust/ash from volcanism may occasionally be deposited at the Lake Pata site, as revealed by the coincident trends observed in the local εNd curve and the WAIS Divide/Antarctica volcanic record during the mid-to-late Holocene.

In summary, our findings indicate that the changes in the radiogenic signal in the Lake Pata sediment record, which includes the last 7.5 kyr B.P., are the result of combined sources modulated by local and global climatic conditions, especially latitudinal shifts, possible width variations and intensification of the ITCZ and the atmospheric dynamics over the southern Atlantic Ocean. Our data, taken from a remote inland site within the Amazon basin, indicates that the Saharan dust influence over the Amazon basin is most likely geographically limited and consequently, that the fertilizing issue cannot be generalized to the entire basin. These conclusions indicate that the fertilization issue of the Amazon rainforest is a more complex multifactorial issue.

Methods

Sediment coring. A lacustrine sediment core, LPTV-09 (0°17′9.68″ N, 66°40′ 36.18″ W), from Lake Pata yielded a detailed record of climatic change during the Holocene, providing a record of the last 7573 years. The coring was conducted in 2009 using a Colinvaux–Vohnout piston corer[37]. The core was sliced into 1-cm layers at the Institut de Recherche pour le Développement (IRD), Bondy, France. Age measurements (of 13 samples) were performed at the Laboratoire de Mesure du Carbone 14 (LMC14)—UMS 2572 (CEA/DSM, CNRS, IRD, IRSN, Ministère de la Culture et de la Communication). Ages were calibrated using the IntCal 13 calibration curve[93] and the chronology curve was constructed using Bacon[94]. Details can be found in Nascimento et al.[29]. Permission for fieldwork #20276-1 at the Neblina National Park was granted by the SISBIO/ICMBIO/MMA/Brazil.

$^{87}Sr/^{86}Sr$ and $^{143}Nd/^{144}Nd$ analysis. The chronology of this core is based upon twelve radiocarbon dates from the retrieved sediment organic matter. The core was sliced into 1-cm intervals and analyzed at 1-10-cm intervals (for a total of 26 samples) for the $^{87}Sr/^{86}Sr$ and $^{143}Nd/^{144}Nd$ isotopic compositions. A TRITON Thermal Ionization Mass Spectrometer (Thermo Scientific) was used at the LAGIR (Laboratory of Geochronology and Radiogenic Isotopes) at UERJ, Rio de Janeiro State University. Additionally, samples of the lateritic crust that forms Lake Pata were also analyzed according to the following analytical procedure.

All chemical procedures were performed in cleanrooms under positive air pressure using HEPA air filters. Acids were twice distilled in sub-boiling mode, and prefiltered and deionized water from a Milli-Q purifier was used. All containers were Teflon made by Savillex. Each sample was weighed (~25 mg) and digested during two cycles: the first one lasted for three days using a mixture of 48% HF and HNO3 6 N (12:1) and the second one lasted for two days using HCl 6 N. The separation and collection of Sr were carried out with HCl 2.5 N and rare-earth elements (REEs) with HCl 6 N using ion-exchange columns filled with Bio-Rad AG50W-X8 (100-200 mesh) cation exchange resin. For the extraction of Nd from the other REEs, a second column with LN Eichrom resin (50–100 μm) was used with HCl 0.18 N. After hot plate evaporation, Sr and Nd were deposited separately onto previously degassed Re filaments in a double-filament setup using 1 μl of H_3PO_4 1 N as the ionization activator. The deposited material was subjected to an initial current of 1.5 A for evaporation of water and acid and then subjected to a current of ~2 A for 3 s to achieve final drying.

The TIMS spectrometric analyses of Sr were performed in static mode, with an arrangement of five Faraday collectors, obtaining a minimum of 100 measurement cycles. The evaporation filament was subjected to a current of 1800–2300 mA, while the ionization filament remained fixed at a current of 3200 mA. For Nd analyses, an array of eight Faraday collectors was used, with a minimum of 160 measurements. The evaporation filament was subjected to a current of 1800–2300 mA, while the ionization filament remained fixed at a current of 4500 mA. The measured $^{87}Sr/^{86}Sr$ and $^{143}Nd/^{144}Nd$ isotopic ratios were normalized using the natural ratios of $^{88}Sr/^{86}Sr = 8.3752$ and $^{146}Nd/^{144}Nd = 0.7219$, respectively. The average $^{87}Sr/^{86}Sr$ ratios for the standard NBS987 and $^{143}Nd/^{144}Nd$ for the JNdi-1 standard in LAGIR are 0.710235 ± 9 and 0.512115 ± 6, respectively. The Nd blanks were below 1000 pg, with an average of 500 pg. For convenience, the $^{143}Nd/^{144}Nd$ ratios are expressed as $\varepsilon Nd(0) = (((^{143}Nd/^{144}Nd/0.512638) - 1) \times 10^4$, expressing deviation from the isotopic ratio of the CHondritic Uniform Reservoir - CHUR[95]. The results are displayed within 2σ analytical uncertainties in Supplementary Data 2.

Sr grain-size effect correction. The grain-size effect is observed in $^{87}Sr/^{86}Sr$ ratios for carbonate-free sediment samples[96]. Thus, to minimize this effect, we applied Sr isotope data correction factors according to the work of Dash[96], Gaiero[97], and Neto[98]. For the North African and Sahara/Sahel sectors, databases were corrected by data from Dash[96], in which we used a factor of 0.0080 for the $^{87}Sr/^{86}Sr$ data (we subtracted this factor from the data). The same procedure was performed on South African data (correction factor of 0.0013). For South America, we used the

Patagonian curve (a factor of 0.0026). For Amazonian soils, we used an average value from the three curves (a factor of 0.0039). This correction was applied to data of bulk sediments or soil samples with grain sizes larger than 50 μm. For the laterite Sr data, no correction was needed since this is a local source. Typical aerosol size modes over the Amazon basin are 1.4 μm for the fine fraction and 7.9 μm for the coarse fraction[88]. The correction values corresponding to the amplitudes of the $^{87}Sr/^{86}Sr$ data taken from 2- and 50-μm grain sizes encompass the maximum variability in grain-size dependence. The results are displayed in Supplementary Fig. 6.

Aerosol analysis. Aerosol filters have a special importance because they allow an isotope signature analysis in the study area before aerosols are deposited and undergo chemical modification. Using isotopic ratio analysis on filters in conjunction with backward air mass trajectories with HYSPLIT (HYbrid Single-Particle Lagrangian Integrated Trajectory)[44,45] and UV aerosol index data[99,100], we can better understand and interpret the aerosol dynamics in the study area. For this approach, one polycarbonate filter and one quartz filter were used for sampling at the Amazon Tall Tower Observatory (ATTO) site, an 80 m-high tower located in the eastern Amazon basin (2°8′38.82″ S, 58°59′59.52″ W), during the wet season in 2012–2013 and the dry season in 2013, respectively. According to Ben-Ami et al.[90], mineral dust takes ~8–12 days to cross the Atlantic Ocean. Thus, the analyses were based on the average AI in the regions of interest (African continent—Atlantic Ocean—South America) 12 days before the aerosol sampling period. Filters were acid digested following the procedures of Gioia et al.[101]: 2 mL (48%) of HF and 0.5 mL of HNO_3 6 N for 3 days at 120–130 °C on a hot plate. Before complete evaporation, we added 1 mL of HNO_3 6 N to ensure that all the HF was eliminated. After evaporation, we added 2 mL of HCl 6 N and heated the solution for two more days under the conditions previously described. Following total evaporation, the extraction of Sr and Nd was carried out as previously described. Sr and Nd isotope results, displayed within 2σ analytical uncertainties, and filter retrieval information can be found in Supplementary Table 1. Two blank aerosol filters of the same type as those used for the ATTO aerosol samples were analyzed. No measurable Nd or Sr signal was observed from the polycarbonate of the filters. In the quartz filter, only the Sr signal was observed, but with low signal intensity.

Potential isotope database sources. Potential source areas of mineral dust exportation to the study site were inferred by a 30-year monthly analysis of backward air mass trajectories using the HYSPLIT/NOAA model available at https://www.ready.noaa.gov/HYSPLIT_traj.php. Trajectories were calculated using the NCEP/NCAR reanalysis database for a 200-h analysis. The coordinates and altitude of Lake Pata were taken as the endpoint of the trajectories, taking into account a model vertical velocity and a mid-boundary layer height. Combined with the Intertropical Convergence Zone (ITCZ) seasonal behavior and based on 39 years of Outgoing Longwave Radiation (OLR) monthly average analysis[102], we obtained a pattern of the air mass trajectories over the Amazon basin reaching its western sector. Finally, extensive literature research was conducted to build a substantial isotope database for these areas to compare with the isotopic results from sediment core LPTV 09 and thus retrieve information on the origin areas of the deposited material. The final database is displayed in Supplementary Data 1.

Binary mixing model. Based on the binary mixture model[56], we have modeled curves for different mixing hypotheses between Seis Lagos hill and a type of isotopic domain value, including an average value, for potential dust source material identified by the backward trajectories. The equation used for the mixture is shown below:

$$R_M^i = \frac{R_A^i X_A f + R_B^i X_B f}{X_A f + X_B (1 - f)},$$

where R is the isotopic ratio for element i, with concentration X of components (end-members) A and B. The f-value in this equation represents the proportion of component A for the mixture M. The complete database used for the mixture curves is provided in Supplementary Data 3 and 4.

Modeled total Saharan aerosol load at Lake Pata. For this estimation, we acquired the modern average dust flux both at the Lake Pata latitude and longitude and at the northern African margin based on the previous models[5,63,64]. We also acquired the dust flux model for the past 6 kyr[64], the Last Glacial Maximum (LGM)[63], and the dust deposition estimation in the North African margin from marine sediment cores[65]. We observed a good correlation ($R^2 = 0.93$) between the estimated aerosol and dust deposited in marine sediment cores, which allowed us to estimate how much of this dust flux would reach the Lake Pata site during the last ~7 kyr. For complementary curves, see Supplementary Fig. 4.

Data availability

The data generated for this paper are available at https://www.ncdc.noaa.gov/paleo-search/study/30893. The authors declare that the data supporting the findings of this study are available within the paper and its supplementary information files.

Received: 21 May 2020; Accepted: 20 November 2020;
Published online: 04 January 2021

References

1. Abouchami, W. et al. Geochemical and isotopic characterization of the bodélé depression dust source and implications for transatlantic dust transport to the Amazon basin. *Earth Planet. Sci. Lett.* **380**, 112–123 (2013).
2. Chin, M., Rood, R. B., Lin, S.-J., Müller, J.-F. & Thompson, A. M. Atmospheric sulfur cycle simulated in the global model GOCART: model description and global properties. *J. Geophys. Res. Atmos.* **105**, 24671–24687 (2000).
3. Cwiertny, D. M., Young, M. A. & Grassian, V. H. Chemistry and photochemistry of mineral dust aerosol. *Annu. Rev. Phys. Chem.* **59**, 27–51 (2008).
4. Haywood, J. Radiative properties and direct radiative effect of Saharan dust measured by the C-130 aircraft during SHADE: 1. Solar spectrum. *J. Geophys. Res.* **108**, 1–16 (2003). SAH 4.
5. Jickells, T. D. et al. Global iron connections between desert dust, ocean biogeochemistry, and climate. *Science* **308**, 67–71 (2005).
6. Kumar, A. et al. A radiogenic isotope tracer study of transatlantic dust transport from Africa to the Caribbean. *Atmos. Environ.* **82**, 130–143 (2014).
7. Maher, B. A. et al. Global connections between aeolian dust, climate and ocean biogeochemistry at the present day and at the last glacial maximum. *Earth Sci. Rev.* **99**, 61–97 (2010).
8. Ozer, P., Laghdaf, M. B. O. M., Lemine, S. O. M. & Gassani, J. Estimation of air quality degradation due to Saharan dust at Nouakchott, Mauritania, from horizontal visibility data. *Water Air Soil Pollut.* **178**, 79–87 (2006).
9. Usher, C. R., Michel, A. E. & Grassian, V. H. Reactions on mineral dust. *Chem. Rev.* **103**, 4883–4939 (2003).
10. Swap, R., Garstang, M., Greco, S., Talbot, R. & Kallberg, P. Saharan dust in the Amazon Basin. *Tellus B* **44**, 133–149 (1992).
11. Reichholf, J. H. Is Saharan dust a major source of nutrients for the Amazonian Rain Forest? *Stud. Neotrop. Fauna Environ.* **21**, 251–255 (1986).
12. Knippertz, P. *Mineral Dust* (Springer, Netherlands, 2014).
13. Aarons, S. M., Aciego, S. M. & Gleason, J. D. Variable HfSrNd radiogenic isotopic compositions in a Saharan dust storm over the Atlantic: Implications for dust flux to oceans, ice sheets and the terrestrial biosphere. *Chem. Geol.* **349–350**, 18–26 (2013).
14. Delmonte, B. et al. Comparing the Epica and Vostok dust records during the last 220,000 years: Stratigraphical correlation and provenance in glacial periods. *Earth Science Rev.* **66**, 63–87 (2004).
15. Grousset, F. E., Rognon, P., Coudé-Gaussen, G. & Pédemay, P. Origins of peri-Saharan dust deposits traced by their Nd and Sr isotopic composition. *Palaeogeogr. Palaeoclimatol. Palaeoecol.* **93**, 203–212 (1992).
16. Yu, H. et al. The fertilizing role of African dust in the Amazon rainforest: a first multiyear assessment based on data from Cloud-Aerosol Lidar and Infrared Pathfinder Satellite Observations. *Geophys. Res. Lett.* 1–8. https://doi.org/10.1002/2015GL063040 (2015).
17. Bristow, C. S., Hudson-Edwards, K. A. & Chappell, A. Fertilizing the Amazon and equatorial Atlantic with West African dust. *Geophys. Res. Lett.* **37**, L14807 (2010).
18. Andreae, M. O. et al. Can Saharan dust explain extensive clay deposits in the Amazon Basin? Radiogenic isotopes as tracers of transatlantic transport. *Mineral. Mag.* **77**, 551–635 (2013).
19. Koren, I. et al. The Bodélé depression: a single spot in the Sahara that provides most of the mineral dust to the Amazon forest. *Environ. Res. Lett.* **1**, 014005 (2006).
20. Haug, G. H. Southward migration of the intertropical convergence zone through the holocene. *Science* **293**, 1304–1308 (2001).
21. Palchan, D. & Torfstein, A. A drop in Sahara dust fluxes records the northern limits of the African humid period. *Nat. Commun.* **10**, 3803 (2019).
22. Formenti, P. et al. Saharan dust in Brazil and Suriname during the large-scale biosphere-atmosphere experiment in Amazonia (LBA) - Cooperative LBA Regional Experiment (CLAIRE) in March 1998. *J. Geophys. Res.* **106**, 14919 (2001).
23. Rizzolo, J. A. et al. Soluble iron nutrients in Saharan dust over the central Amazon rainforest. *Atmos. Chem. Phys.* **17**, 2673–2687 (2017).
24. Ben-Ami, Y. et al. Transport of Saharan dust from the Bodélé Depression to the Amazon Basin: a case study. *Atmos. Chem. Phys. Discuss.* **10**, 4345–4372 (2010).
25. Köppen, Wladimir, Geiger, R. *Handbuch der Klimatologie: Das geographische System der Klimate* (Verlag von Gebrüder Borntraeger, 1936).
26. Kottek, M., Grieser, J., Beck, C., Rudolf, B. & Rubel, F. World map of the Köppen-Geiger climate classification updated. *Meteorol. Zeitschrift* **15**, 259–263 (2006).

27. Bush, M. B., De Oliveira, P. E., Colinvaux, P. A., Miller, M. C. & Moreno, J. E. Amazonian paleoecological histories: one hill, three watersheds. *Palaeogeogr. Palaeoclimatol. Palaeoecol.* **214**, 359–393 (2004).
28. Bush, M. B. et al. Holocene fire and occupation in Amazonia: records from two lake districts. *Philos. Trans. R. Soc. Lond. B Biol. Sci.* **362**, 209–218 (2007).
29. Nascimento, M. N. et al. Vegetation response to climatic changes in western Amazonia over the last 7,600 years. *J. Biogeogr.* **46**, 2389–2406 (2019).
30. Bush, M. B., Miller, M. C., De Oliveira, P. E. & Colinvaux, P. A. Orbital forcing signal in sediments of two Amazonianlakes. *J. Paleolimnol* **27**, 341–352 (2002).
31. Cordeiro, R. C. et al. Biogeochemical indicators of environmental changes from 50Ka to 10Ka in a humid region of the Brazilian Amazon. *Palaeogeogr. Palaeoclimatol. Palaeoecol.* **299**, 426–436 (2011).
32. Santos, G. M. et al. Chronology of the atmospheric mercury in Lagoa Da Pata Basin upper Rio Negro region of Brazilian Amazon. *Radiocarbon* **43**, 801–808 (2001).
33. Barbosa, J. et al. 14C-AMS as a tool for the investigation of mercury deposition at a remote Amazon location. *Nucl. Instrum. Methods Phys. Res. Sect. B Beam Interact. Mater. Atoms* **223–224**, 528–534 (2004).
34. Van Der Hammen, T. & Hooghiemstra, H. Neogene and quaternary history of vegetation, climate, and plant diversity in Amazonia. *Quat. Sci. Rev.* **19**, 725–742 (2000).
35. Anhuf, D. et al. Paleo-environmental change in Amazonian and African rainforest during the LGM. *Palaeogeogr. Palaeoclimatol. Palaeoecol.* **239**, 510–527 (2006).
36. D'Apolito, C., Absy, M. L. & Latrubesse, E. M. The Hill of Six Lakes revisited: new data and re-evaluation of a key Pleistocene Amazon site. *Quat. Sci. Rev.* **76**, 140–155 (2013).
37. Colinvaux, P. A., de Oliveira, P. E., Moreno, J. E., Miller, M. C. & Bush, M. B. A long pollen record from lowland Amazonia: forest and cooling in glacial times. *Science* **274**, 85–88 (1996).
38. Grousset, F. E. et al. Antarctic (Dome C) ice-core dust at 18 k.y. B.P.: isotopic constraints on origins. *Earth Planet. Sci. Lett.* **111**, 175–182 (1992).
39. Grousset, F. E. & Biscaye, P. E. Tracing dust sources and transport patterns using Sr, Nd and Pb isotopes. *Chem. Geol.* **222**, 149–167 (2005).
40. Basile, I. et al. Patagonian origin of glacial dust deposited in East Antarctica (Vostok and Dome C) during glacial stages 2, 4 and 6. *Earth Planet. Sci. Lett.* **146**, 573–589 (1997).
41. Delmonte, B. et al. Aeolian dust in the Talos Dome ice core (East Antarctica, Pacific/Ross Sea sector): Victoria Land versus remote sources over the last two climate cycles. *J. Quat. Sci.* **25**, 1327–1337 (2010).
42. Delmonte, B. et al. Modern and Holocene aeolian dust variability from Talos Dome (Northern Victoria Land) to the interior of the Antarctic ice sheet. *Quat. Sci. Rev.* **64**, 76–89 (2013).
43. Prospero, J. M., Glaccum, R. A. & Nees, R. T. Atmospheric transport of soil dust from Africa to South America. *Nature* **289**, 570–572 (1981).
44. Rolph, G., Stein, A. & Stunder, B. Real-time environmental applications and display sYstem: READY. *Environ. Model. Softw.* **95**, 210–228 (2017).
45. Stein, A. F. et al. NOAA's HYSPLIT atmospheric transport and dispersion modeling system. *Bull. Am. Meteorol. Soc* **96**, 2059–2077 (2015).
46. Alonso-Pérez, S., Cuevas, E., Querol, X., Guerra, J. C. & Pérez, C. African dust source regions for observed dust outbreaks over the Subtropical Eastern North Atlantic region, above 25°N. *J. Arid Environ.* **78**, 100–109 (2012).
47. Zielhofer, C. et al. Millennial-scale fluctuations in Saharan dust supply across the decline of the African Humid Period. *Quat. Sci. Rev.* **171**, 119–135 (2017).
48. Escudero, M. et al. Determination of the contribution of northern Africa dust source areas to PM10 concentrations over the central Iberian Peninsula using the Hybrid Single-Particle Lagrangian Integrated Trajectory model (HYSPLIT) model. *J. Geophys. Res.* **111**, D06210 (2006).
49. McGowan, H. & Clark, A. Identification of dust transport pathways from Lake Eyre, Australia using Hysplit. *Atmos. Environ.* **42**, 6915–6925 (2008).
50. Perry, K. D., Cahill, T. A., Eldred, R. A., Dutcher, D. D. & Gill, T. E. Long-range transport of North African dust to the eastern United States. *J. Geophys. Res.* **102**, 225–238 (1997).
51. Prospero, J. M. Long-term measurements of the transport of African mineral dust to the southeastern United States: implications for regional air quality. *J. Geophys. Res. Atmos.* **104**, 15917–15927 (1999).
52. Cabos, W. et al. The South Atlantic Anticyclone as a key player for the representation of the tropical Atlantic climate in coupled climate models. *Clim. Dyn.* **48**, 4051–4069 (2017).
53. Lupo, A. R., Nocera, J. J., Bosart, L. F., Hoffman, E. G. & Knight, D. J. South American cold surges: types, composites, and case studies. *Mon. Weather Rev.* **129**, 1021–1041 (2001).
54. Reinke, R. Das Klima Amazoniens. Dissertation, University of Tübingen, 1962.
55. Kumar, A. et al. Seasonal radiogenic isotopic variability of the African dust outflow to the tropical Atlantic Ocean and across to the Caribbean. *Earth Planet. Sci. Lett.* **487**, 94–105 (2018).
56. Faure, G. *Principles of Isotope Geology* (Wiley, 1986).
57. Kaufman, Y. J. et al. Dust transport and deposition observed from the Terra-Moderate Resolution Imaging Spectroradiometer (MODIS) spacecraft over the Atlantic Ocean. *J. Geophys. Res. D Atmos.* **110**, 1–16 (2005).
58. Talbot, R. W. et al. Aerosol chemistry during the wet season in Central Amazonia: the influence of long-range transport. *J. Geophys. Res.* **95**, 16955–16969 (1990).
59. Hawkesworth, C. J. et al. 143Nd/144Nd,87Sr/86Sr, and incompatible element variations in calc-alkaline andesites and plateau lavas from South America. *Earth Planet. Sci. Lett.* **42**, 45–57 (1979).
60. Kurbatov, A. V. et al. A 12,000 year record of explosive volcanism in the Siple Dome Ice Core, West Antarctica. *J. Geophys. Res.* **111**, D12307 (2006).
61. Cole, J. M., Goldstein, S. L., deMenocal, P. B., Hemming, S. R. & Grousset, F. E. Contrasting compositions of Saharan dust in the eastern Atlantic Ocean during the last deglaciation and African Humid Period. *Earth Planet. Sci. Lett.* **278**, 257–266 (2009).
62. Skonieczny, C. et al. African humid periods triggered the reactivation of a large river system in Western Sahara. *Nat. Commun.* **6**, 6–11 (2015).
63. Muhs, D. R., Budahn, J. R., Prospero, J. M., Skipp, G. & Herwitz, S. R. Soil genesis on the island of Bermuda in the quaternary: the importance of African dust transport and deposition. *J. Geophys. Res. Earth Surf.* **117**, 1–26 (2012).
64. Egerer, S., Claussen, M., Reick, C. & Stanelle, T. The link between marine sediment records and changes in Holocene Saharan landscape: simulating the dust cycle. *Clim. Past* **12**, 1009–1027 (2016).
65. McGee, D., deMenocal, P. B., Winckler, G., Stuut, J. B. W. & Bradtmiller, L. I. The magnitude, timing and abruptness of changes in North African dust deposition over the last 20,000 yr. *Earth Planet. Sci. Lett.* **371–372**, 163–176 (2013).
66. Shanahan, T. M. et al. The time-transgressive termination of the African humid period. *Nat. Geosci.* **8**, 140–144 (2015).
67. Prado, L. F., Wainer, I., Chiessi, C. M., Ledru, M.-P. & Turcq, B. Mid-Holocene climate reconstruction for eastern South America. *Clim. Past Discuss.* **8**, 5925–5961 (2012).
68. Absy, M. L. et al. Mise en évidence de quatre phase d'ouverture de la forêt dens le sud-est de l'Amazonie au cours des 60000 derniéres années. Première comparaison avec d'autres régions tropicales. *C. R. Acad. Sci. Paris* **2**, 673–678 (1991).
69. Mayle, F. E. & Power, M. J. Impact of a drier Early-Mid-Holocene climate upon Amazonian forests. *Philos. Trans. R. Soc. Lond. B Biol. Sci.* **363**, 1829–1838 (2008).
70. Sifeddine, A. et al. Variations of the Amazonian rainforest environment: a sedimentological record covering 30,000 years. *Palaeogeogr. Palaeoclimatol. Palaeoecol.* **168**, 221–235 (2001).
71. McGee, D., Donohoe, A., Marshall, J. & Ferreira, D. Changes in ITCZ location and cross-equatorial heat transport at the Last Glacial Maximum, Heinrich Stadial 1, and the mid-Holocene. *Earth Planet. Sci. Lett.* **390**, 69–79 (2014).
72. Shimizu, M. H., Sampaio, G., Venancio, I. M. & Maksic, J. Seasonal changes of the South American monsoon system during the Mid-Holocene in the CMIP5 simulations. *Clim. Dyn.* **54**, 2697–2712 (2020).
73. deMenocal, P. et al. Abrupt onset and termination of the African Humid Period: rapid climate responses to gradual insolation forcing. *Quat. Sci. Rev* **19**, 347–361 (2000).
74. Kropelin, S. et al. Climate-driven ecosystem succession in the Sahara: the past 6000 years. *Science (80-)* **320**, 765–768 (2008).
75. Ritchie, J. C., Eyles, C. H. & Haynes, C. V. Sediment and pollen evidence for an early to mid-Holocene humid period in the eastern Sahara. *Nature* **314**, 352–355 (1985).
76. Tyson, P. D. Late-Quaternary and Holocene palaeoclimates of southern Africa: a synthesis. *South Afr. J. Geol.* **102**, 335–349 (1999).
77. Thomas, D. S. G., Stokes, S. & Shaw, P. A. Holocene aeolian activity in the southwestern Kalahari Desert, southern Africa: significance and relationships to late-pleistocene dune-building events. *Holocene* **7**, 273–281 (1997).
78. Wanner, H. et al. Mid- to Late Holocene climate change: an overview. *Quat. Sci. Rev.* **27**, 1791–1828 (2008).
79. Farmer, E. C., deMenocal, P. B. & Marchitto, T. M. Holocene and deglacial ocean temperature variability in the Benguela upwelling region: implications for low-latitude atmospheric circulation. *Paleoceanography* **20**, 1–16 (2005).
80. Wündsch, M. et al. Holocene environmental change along the southern Cape coast of South Africa – Insights from the Eilandvlei sediment record spanning the last 8.9 kyr. *Glob. Planet. Change* **163**, 51–66 (2018).
81. Cheng, H. et al. Climate change patterns in Amazonia and biodiversity. *Nat. Commun.* **4**, 1411 (2013).
82. Apaéstegui, J. et al. Hydroclimate variability of the northwestern Amazon Basin near the Andean foothills of Peru related to the South American Monsoon System during the last 1600 years. *Clim. Past* **10**, 1967–1981 (2014).
83. Silva Dias, P. L., Turcq, B., Silva Dias, M. A. F., Braconnot, P. & Jorgetti, T. in *Past Climate Variability in South America and Surrounding Regions* Vol. 14 (eds Francoise, V., Sylvestre, Florence, S. & Myriam, K.) 259–281 (Springer, 2009).

84. Forti, M. C. & Moreira-Nordemann, L. M. Rainwater and throughfall chemistry in a Terra Firme rain-forest - Central Amazonia. *J. Geophys. Res.* **96**, 7415–7421 (1991).
85. Jordan, C. F. The nutrient balance of an Amazonian rain forest. *Ecology* **63**, 647–654 (1982).
86. Arana, A. & Artaxo, P. Elemental composition of the atmospheric aerosol in the central amazon basin. *Quim. Nova* **37**, 268–276 (2014).
87. Artaxo, P. et al. Aerosol particles in Amazonia: their composition, role in the radiation balance, cloud formation, and nutrient cycles. *Geophys. Monogr. Ser.* https://doi.org/10.1029/2008GM000778 (2009).
88. Artaxo, P. et al. Atmospheric aerosols in Amazonia and land use change: from natural biogenic to biomass burning conditions. *Faraday Discuss* **165**, 203–235 (2013).
89. Worobiec, A. et al. Characterisation of Amazon Basin aerosols at the individual particle level by X-ray microanalytical techniques. *Atmos. Environ.* **41**, 9217–9230 (2007).
90. Ben-Ami, Y. et al. Transport of North African dust from the Bodélé depression to the Amazon Basin: a case study. *Atmos. Chem. Phys.* **10**, 7533–7544 (2010).
91. Okin, G. S., Mahowald, N., Chadwick, O. A. & Artaxo, P. Impact of desert dust on the biogeochemistry of phosphorus in terrestrial ecosystems. *Global Biogeochem. Cycles* **18**, GB2005 (2004).
92. Prospero, J. M. et al. Characterizing and quantifying African dust transport and deposition to South America: implications for the phosphorus budget in the Amazon Basin. *Global Biogeochem. Cycles* **34**, e2020GB006536 (2020).
93. Reimer, P. J. et al. IntCal13 and Marine13 radiocarbon age calibration curves 0–50,000 years cal BP. *Radiocarbon* **55**, 1869–1887 (2013).
94. Blaauw, M. & Christeny, J. A. Flexible paleoclimate age-depth models using an autoregressive gamma process. *Bayesian Anal.* https://doi.org/10.1214/11-BA618 (2011).
95. DePaolo, D. J. & Wasserburg, G. J. Nd isotopic variations and petrogenic models. *Geophys. Res. Lett.* **3**, 249–252 (1976).
96. Dasch, E. J. Strontium isotopes in weathering profiles, deep-sea sediments, and sedimentary rocks. *Geochim. Cosmochim. Acta* **33**, 1521–1552 (1969).
97. Gaiero, D. M. Dust provenance in Antarctic ice during glacial periods: from where in southern South America? *Geophys. Res. Lett.* **34**, 1–6 (2007).
98. Neto, C. C. A. *Caracterização Isotópica (Nd-Sr) E Litogeoquímica De Sedimentos Atuais Da Namíbia (África): Implicações Para Proveniência Sedimentar E Potencial Fonte De Aerossol* (Universidade do Estado do Rio de Janeiro, 2018).
99. Acker, J. G. & Leptoukh, G. Online analysis enhances use of NASA earth science data. *Eos Trans. Am. Geophys. Union* **88**, 14 (2007).
100. Bhartia, P. K. OMI/Aura TOMS-Like Ozone, Aerosol Index, Cloud Radiance Fraction L3 1 day 1 degree x 1 degree V3, NASA Goddard Space Flight Center, Goddard Earth Sciences Data and Information Services Center (GES DISC), https://doi.org/10.5067/Aura/OMI/DATA3001 (2012).
101. Gioia, S. M. C. L., Babinski, M., Weiss, D. J. & Kerr, A. A. F. S. Insights into the dynamics and sources of atmospheric lead and particulate matter in São Paulo, Brazil, from high temporal resolution sampling. *Atmos. Res.* **98**, 478–485 (2010).
102. Liebmann, B. & Smith, C. A. Description of a complete (interpolated) outgoing longwave radiation datasets. *Bull. Amer. Meteor. Soc.* **77**, 1275–1277 (1996).
103. Schneider, U. et al. *GPCC Full Data Reanalysis Version 6.0 at 0.5°: Monthly Land-Surface Precipitation from Rain-Gauges Built on GTS-Based and Historic Data*. https://doi.org/10.3390/atmos8030052 (GPCC, 2011).

Acknowledgements

This study was financed in part by the *Conselho Nacional de Desenvolvimento Científico e Tecnológico* (CNPq), Brazil—for the field excursion and analysis—and by the *Coordenação de Aperfeiçoamento de Pessoal de Nível Superior* (CAPES), Brazil—who provided the main author with a master's scholarship during the development of this work. Thanks are also due to Dr. Nivaldo Ferreira (Universidade Estadual do Norte Fluminense – UENF) for his valuable advice on the OLR data analysis and to Dr. Mark Bush for his support on the field mission. We acknowledge the National Oceanic and Atmospheric Administration (NOAA) Air Resources Laboratory (ARL) for the provision of the HYSPLIT transport and dispersion model and READY website (http://www.ready.noaa.gov). We also thank Victoria Barros and Leonardo Monteiro for their support. C. Valeriano acknowledges the CNPq and FAPERJ Brazilian funding agencies for scholarship and research grants.

Author contributions

This work was a result of J.N. master's dissertation; therefore, J.N. contributed to this manuscript by constructing the Sr/Nd database of potential sources, determining the ITCZ historical positions through OLR data, performing the analysis and statistical validation of the results, simulating the backward air mass trajectories, estimating the dust flux, preparing all of the figures and finally writing, and structuring the main manuscript text. H.E. contributed to the writing of the main manuscript text, the climatic mechanism discussion, and the major revision and supervision during the realization of this work. C.V. contributed to the discussion and application of the Sr/Nd method, prepared the correct methodology to apply to our specific matrix, and contributed to the writing of the main manuscript text. A.S. contributed to the sediment core acquisition, the climatic mechanism discussion, and the writing and structuring of the written document. C.N. performed the radiogenic isotope analysis. G.V. performed all of the chemical pretreatments for both the sediment and the filter samples analyzed for radiogenic isotopes. L.M. contributed to the discussion on the Amazonian climate and the interpretation of the results. R.C. contributed to the sediment core acquisition and climatic mechanism discussion. A.B. provided the Seis Lagos hill lateritic crust samples for the Sr/Nd analysis. G.M. and K.A. contributed to the sedimentology description, the preparation of the samples for organic analysis, and the sediment dating. R.G. provided the ATTO filters for the methodology validation and the major revision of this text. B.T. planned and provided funding for the realization of both fieldworks for core extraction at the study site and radiocarbon analysis. C.B. contributed to the sampling and handling of the aerosol filters at the ATTO. Finally, M.S. was responsible for the climatic simulations with CMIP5 and revision of the manuscript text.

Competing interests

The authors declare no competing interests.

Additional information

Supplementary information is available for this paper at https://doi.org/10.1038/s43247-020-00071-w.

Correspondence and requests for materials should be addressed to J.N.

Peer review information Primary handling editors: Rachael Rhodes, Heike Langenberg

Reprints and permission information is available at http://www.nature.com/reprints

Publisher's note Springer Nature remains neutral with regard to jurisdictional claims in published maps and institutional affiliations.